Progress in Natural Science: Materials International 26 (2016) 613–620

HOSTED BY

Contents lists available at ScienceDirect

Progress in Natural Science: Materials International

journal homepage: www.elsevier.com/locate/pnsmi

Original Research

Cu-$(B_4C)_p$ metal matrix composites processed by accumulative roll-bonding

S. Mansourzadeh[a,*], M. Hosseini[b], E. Salahinejad[c,*], A.H. Yaghtin[a]

[a] Department of Materials Science and Engineering, College of Chemical and Metallurgical Engineering, Shiraz Branch, Islamic Azad University, Shiraz 71955, Iran
[b] Department of Materials Science and Engineering, School of Engineering, Shiraz University, Shiraz, Iran
[c] Faculty of Materials Science and Engineering, K.N. Toosi University of Technology, Tehran, Iran

ARTICLE INFO

Keywords:
Electron microscopy
Mechanical characterization
Composites

ABSTRACT

In this study, Cu/B_4C metal matrix composites were prepared by accumulative roll-bonding (ARB). The microstructure of the processed samples was characterized by TEM, SEM and optical microscopy. The microhardness, uniaxial tensile and four-point probe tests were carried out to evaluate the mechanical properties and electrical resistivity of the ARBed monolithic and composite samples. The results showed that the reinforcement distribution was improved by increasing ARB cycles, which was quantitatively confirmed by some models. Based on TEM observations, the formation of an ultrafine grained structure in the composite matrix was also approved. It was shown that with increasing ARB cycles, the microhardness and tensile strength of the monolithic Cu samples were enhanced up to the 3rd cycle and then saturated, but the microhardness and tensile strength of the composites showed an increasing trend to the last cycle. Apart from a substantial improvement in the mechanical properties of the Cu/B_4C composites, a minor decrement in electrical conductivity was detected after six ARB cycles.

1. Introduction

Copper (Cu) is one of the most industrially applicable metals due to its especial properties like high ductility, suitable corrosion resistance, and good thermal and electrical conductivity. Although various applications have been developed for Cu, this metal is mainly used as an electrical conductor (over 60%) [1]. Similar to other high-conductive metals, commercially pure Cu is relatively soft. However, in some especial applications like contactors, switches and conductive springs, high electrical conductivity in addition to high mechanical strength are the basic material requirements. There are five main methods to strengthen metallic materials, including precipitation, solid solution, strain, grain boundary, and dispersion hardening techniques [2]. The first two methods are based on the addition of especial alloying elements to the metal. Though the mechanical properties of a metallic material can be improved, the electrical conductivity will be severely degraded synchronously. For instance, in the case of Cu, the addition of alloying elements could increase its tensile strength by 200–300%, but it enhances electrical resistivity (ER) up to tenfold at the same time [3]. However, it has been shown that the application of the other strengthening methods (i.e. strain, grain boundary and dispersion hardening) has minor impacts on electrical resistivity of Cu [4-6]. Therefore, the grain boundary and dispersion hardening techniques seem to be promising for the fabrication of high-strength, high-conductive Cu-based materials.

Various methods have been suggested to produce high-strength, high-conductive materials. Generally, the sub-categories of severe plastic deformation (SPD) techniques such as equal channel angular extrusion (ECAE) [7], accumulative roll bonding (ARB) [5] and high pressure torsion (HPT) [8], have been used to process high-strength, high-conductive nanocrystalline (NC)/ultrafine grained (UFG) Cu alloys. SPD is a top-down economical approach which refines the microstructure of metallic materials by the development of crystallographic defects like dislocation cells and grain boundaries [9]. On the other hand, powder metallurgy, liquid infiltration, plasma spray, deposition, in-situ reaction and ARB processes are some of the main manufacturing methods of Cu matrix composite materials. Hereon, ARB is a mutual method which could be used to strengthen the metallic material via strain, grain boundary and dispersion hardening mechanisms simultaneously [10,11]. This is due to the fact that rolling is not only a deformation process, but also is a joining approach of neighboring metallic layers, as inferred from the process name. The other

Peer review under responsibility of Chinese Materials Research Society.
* Corresponding authors.
E-mail addresses: sh.mansourzadeh@gmail.com (S. Mansourzadeh), salahinejad@kntu.ac.ir, erfan.salahinejad@gmail.com (E. Salahinejad).

http://dx.doi.org/10.1016/j.pnsc.2016.11.006
Received 5 May 2016; Received in revised form 17 August 2016; Accepted 9 November 2016
Available online 09 December 2016
1002-0071/

advantages of ARB are the high rate of production, elimination of structural porosities owing to applied compression and shear stresses, non-limited content of the produced material, and no need for expensive and high load capacity forming facilities. These benefits make ARB a promising technique to fabricate NC/UFG metal matrix composite materials.

Boron carbide (B_4C), which is called "black diamond", is a robust super hard ceramic (third hardest material known, after diamond and cubic boron nitride) [12]. Moreover, it has high cross section for neutrons absorption and is stable against ionizing radiation as well [13]. In previous studies, the ARB production, microstructure and properties of aluminum matrix composites reinforced by B_4C particulates as a high-strength, light-weight material have been extensively investigated [14-18]. However, to our knowledge, no work has been reported on the characterization of Cu/B_4C composite materials fabricated by the ARB process. It should be mentioned that this composite has been previously produced by different techniques. Bai et al. [19] produced this composite by electroless deposition and reported its high thermal conductivity. In another investigation, various Cu matrix particulate reinforced surface composites have been fabricated by friction stir processing [20]. The results indicated that the highest microhardness and lowest wear rate were observed for the B_4C reinforced composites. Powder metallurgy has been also employed to produce Cu/B_4C composites. It has been reported that the hardness of the composites is improved by increasing the B_4C content [21].

The aim of the current study is the production of Cu/B_4C composites as high-strength, high-conductive materials via ARB process. Then, the structure and some properties of the produced composites are investigated.

2. Materials and experimental procedures

2.1. Sample preparation

Commercially pure Cu alloy (C11000) strips in the dimensions of 80×50×0.2 mm^3 (length×width×thickness) and B_4C powders with an average size of 6 μm were used as the raw materials. In order to fabricate Cu-4 vol% B_4C composites, five Cu strips were degreased in acetone and then scratch brushed via a stainless steel round wire brush. Then, they were stacked over each other to achieve 1 mm thickness, while 1 vol% B_4C powders were dispersed between each pair of the strips using a sieve. To prevent the Cu layers from sliding during the roll bonding process, they were fastened at both ends by aluminum wires. Afterwards, the first stage of the process was carried out with a draft percentage of 66% reduction to ensure the creation of a proper bond between the adjacent layers. It should be mentioned that in the first roll-bonding step, the ceramic particles within the interfaces act as a barrier against joining, and consequently the rolling reduction should be enhanced to overcome it. Afterwards, the 0.33 mm sample was longitudinally divided into two equal parts, surface prepared (degreasing and scratch brushing), stacked over each other and then roll-bonded by 50% reduction in thickness (the second step of the roll-bonding process). The second step of the roll-bonding step continued to fabricate six cycles ARB-processed Cu/B_4C composites. The rolling processes were carried out at the ambient temperature and at a rolling speed of 6 rpm in the dry condition. The schematic illustration of the process to produce the Cu/B_4C composites is displayed in Fig. 1.

2.2. Microstructure evaluation

The microstructure characterization of the produced composites was accomplished using an optical microscope (OM). The samples were cut and polished along the rolling direction normal to plane using different grit size sandpapers, and finally by a fine alumina suspension. Etching was performed using a mixture of 2 g potassium dichromate, 8 ml sulfuric acid, 4 drops of the hydrochloric acid solution and 100 ml distilled water.

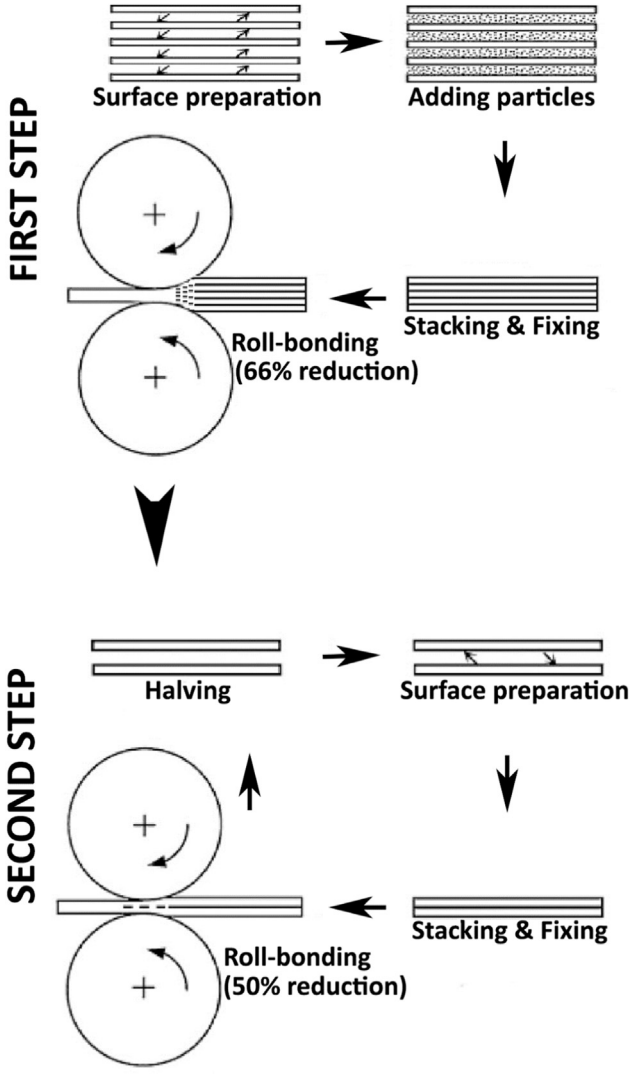

Fig. 1. Schematic illustration of the Cu/B_4C composite production via the ARB process.

The distribution of the B_4C particles within the Cu matrix was quantified by the radial distribution function [11,18]. In this method, a circle of radius r is centered on a particle and the function $H(r)$ is defined as:

$$H(r) = \frac{N_{ra}}{N_a} \quad (1)$$

where N_{ra} and N_a are the number of the particles within the disc area (having the radius of r) and the mean number of the particles over the whole sample, respectively. In the fully random particle distribution, the $H(r)$ function has a constant value of 1. On the other hand, if the particles distribution was extremely clustered, this function displays severe undulations before approaching 1 by increasing the disc radii. The area A_H shows the degree of clustering, as calculated by the deviation of the experimental $H(r)$ curves from $H(r)$ =1. These functions were expressed by:

$$H(r) = ae^{-br} + c \quad (2)$$

$$A_H = \int_{r=20\ \mu m}^{r=120\ \mu m} [H(r)-1]dr \quad (3)$$

where a, b, and c are constants. In the current research a range of radii from r =20 μm to r =120 μm was selected in order to determine the radial distribution function.

A scanning electron microscope (SEM) was used to study the fracture surface of the ruptured tensile test specimens. The matrix microstructure was investigated using a transmitted electron microscope (TEM). The specimen preparation for the TEM analysis was carried out via mechanical polishing followed by ion-milling.

2.3. Mechanical and electrical resistivity properties tests

Uniaxial tensile and Vickers microhardness tests were employed to evaluate the mechanical properties of the materials. Dog-bone shaped tensile test specimens were extracted from the ARBed samples along RD using an electric discharge machine. The specimen dimensions were according to 4/25 scale of JIS no. 5 standard. The tensile tests were performed at room temperature and an initial strain rate of $5\times10^{-3}\ s^{-1}$. The microhardness tests were carried out on the RD-ND plane of the specimens under a load of 50 g and a dwell time of 15 s. The reported microhardness values were the average of 10 separated measurements taken at randomly selected locations.

The standard four-point probe direct current technique was used to measure electrical resistivity of the samples at room temperature. In each case, three resistivity measurements were carried out. More details about this method and specimen dimension are presented elsewhere [22].

3. Results and discussion

Fig. 2 shows the cross-section image of the specimens processed at different cycles. It was found that in the two-cycle processed composite (C2) the ceramic particles were densely localized between the metallic layers. By increasing ARB cycles to three, the thickness of the agglomerated ceramic particle was bundled and their side distance decreased. Moreover, the presence of isolated metallic layers was obvious, although the reinforcement distribution was improved to some extent. When the number of the Cu layers increased to 40 and 80 in the C4 and C5 samples, the recognition of discrete metallic layers becomes difficult. Nonetheless, the small and localized particle agglomerated zones still existed in these samples. The high-magnification OM micrograph of the C4 specimen illustrates a typical location of such zones, as shown in Fig. 3a. Regarding Fig. 2e, it can be stated that the gradual improvement of the reinforcement distribution by continuing the ARB process finally resulted in uniformly-dispersed B_4C particles within the Cu matrix in the C6 specimen. This composite contains 160 metallic layers with a mean thickness of 2 μm which is even smaller than the average particle size of B_4C.

It is believed that the mechanism of the particle distribution evolution is mainly based on the matrix plastic flow. In the initial ARB cycles the ceramic particles were embedded within large interfacial bundles. Although these bundles deformed during the rolling process, their induced deformation strain was lower than the metallic matrix. The extrusion of the interfacial virgin metals and the formation

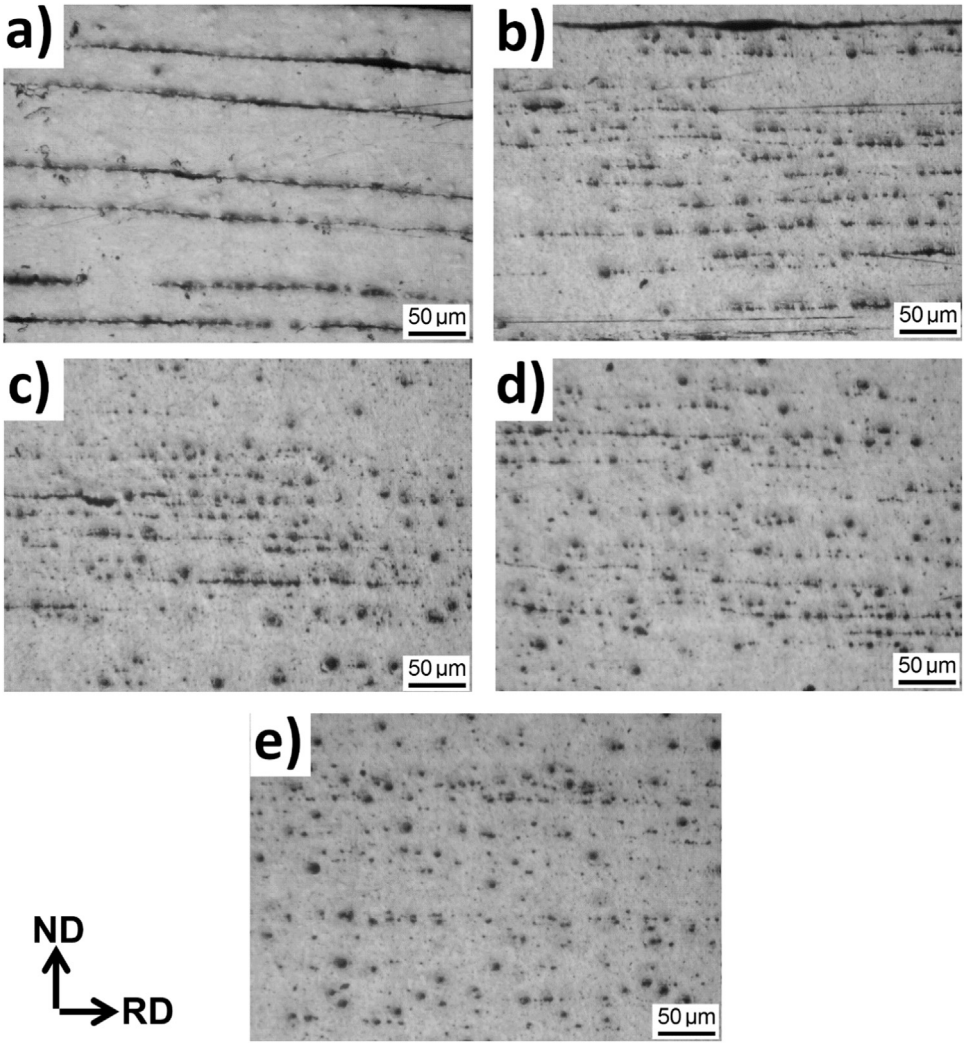

Fig. 2. OM micrographs of the composite samples processed to (a) two, (b) three, (c) four, (d) five and (e) six ARB cycles.

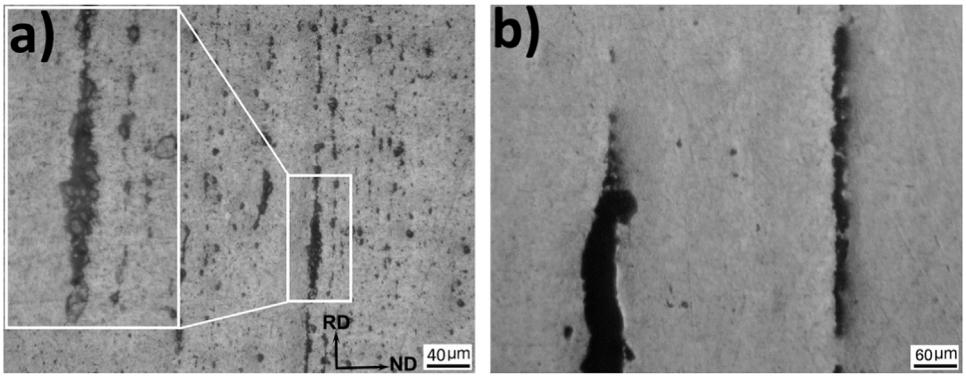

Fig. 3. High-magnification OM images of the Cu/B_4C composites processed to (a) four and (b) two ARB cycles.

of shear bands in Cu by increasing ARB cycles could fragment the ceramic bundles, improving the reinforcement distribution. It has been shown that the appearance of shear bands (non-crystallographic deformation) by increasing the deformation cycles in Cu (or other low to medium stacking fault energy metals) is due to the increment of the dislocation density and consequently the inhibition of homogeneous dislocation slip (crystallographic deformation) [23,24]. It has been frequently reported that in ARB processing of bimetal multilayered composites, the formation of shear bands is the main reason of harder layer plastic instability and finally fragmentation [25,26]. The differences in the deformability (ability to receive strain) of the matrix and reinforcement fragmented bundles result in the creation of a relative flow of the matrix with respect to the ceramic bundles. The particles placed adjacent to the bundle/matrix interfaces are less constrained in comparison with inner particles and therefore they detached and outflowed by tumbling along the interface. The gradual particle separation as well as layer thinning by increasing the cyclic deformation lead to a uniform dispersion of the B_4C particles within the matrix lastly.

The radial distribution function ($H(r)$) of the C2 to C6 composites is plotted in Fig. 4. As it can be seen, although all the curves approach 1 by increasing the radius, the variation domain was reduced by increasing ARB cycles. The undulatory shape of the curves is owing to the layered dispersion of the particles between the Cu sheets. By increasing the radius the transition of the hypothetical disc through a ceramic layer or bundle considerably changes the N_{ra}; and consequently, a sharp change appeared in the corresponding diagram. The elimination of the ceramic agglomeration bundles by continuing ARB reduces the diagram variation, which is a remarkable sign of a uniform particles distribution. Fig. 5 demonstrates the degree of clustering (A_H) at various ARB cycles. The decreasing trend of A_H by continuing the ARB process quantitatively confirms the qualitative improvement of

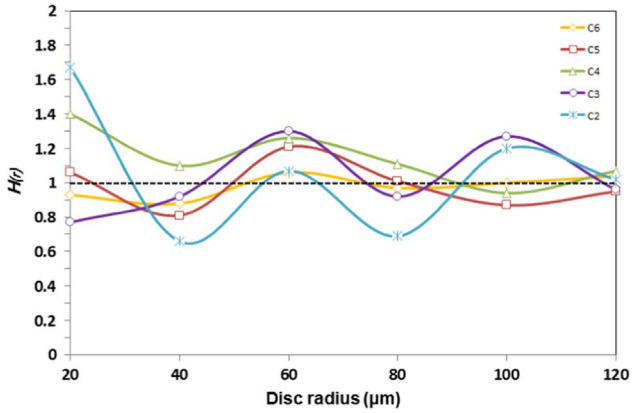

Fig. 4. Radial distribution function plots of the Cu/B_4C composites fabricated from two to six ARB cycles, as nominated C2 to C6.

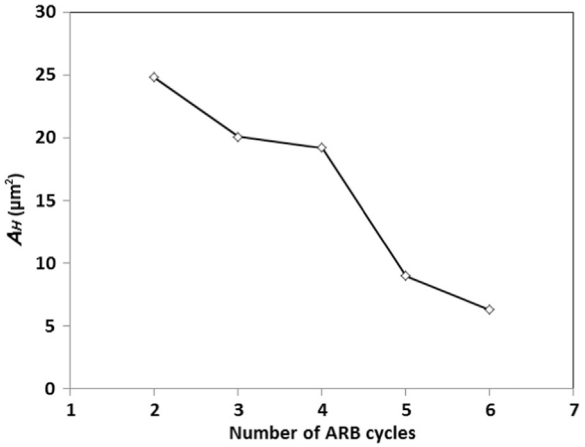

Fig. 5. Degree of clustering of the processed composites.

the particles distribution within the matrix (Fig. 2). The significant decrement of A_H from 25 (C2) to 7 (C6) μm^2 shows the ability of the ARB process to produce a metal matrix composite with a homogenous structure.

Reihanian et al. [27] proposed models to predict the critical reduction (deformation cycle) required to achieve a homogeneous particle distribution in a particulate reinforced metal matrix composite fabricated by ARB. Regarding the models, the total reduction of the composite should be higher than a critical reduction in each SC, BCC and FCC particle distribution configurations in order to ensure the particles distribution uniformity. Hereon, the critical reductions corresponding to the SC, BCC and FCC distribution configurations are 0.929, 0.923 and 0.920, respectively. Also, the total reductions after 2, 3, 4, 5 and 6 cycles are approximately 0.84, 0.92, 0.96, 0.98 and 0.99, respectively. Therefore, the model predicts a uniform B_4C particles distribution after four ARB cycles of processing. However, direct observations confirm the structural homogeneity after six cycles. It seems that this nonconformity originates from some model simplifications. For instance, due to particles crushing during the ARB process [28], the average particle size is not constant and is reduced after each cycle. The nonhomogeneous deformations of the matrix (owing to the shear band formation) and ceramic bundles with respect to the matrix as well as the non-perfect plain strain deformation mode of the samples (~10% of sample broadening after each cycle) are some existing phenomena in the ARB, which are not considered in the model. Generally, it can be stated that the critical strains assessed by the models are just prerequisite deformation values to attain a uniform particles distribution in a particulate reinforced metal matrix composite fabricated by ARB.

The microstructures of the composite's matrix in the annealed condition as well as after six ARB cycles are displayed in Fig. 6. The average grain sizes of the annealed and six-cycles processed Cu

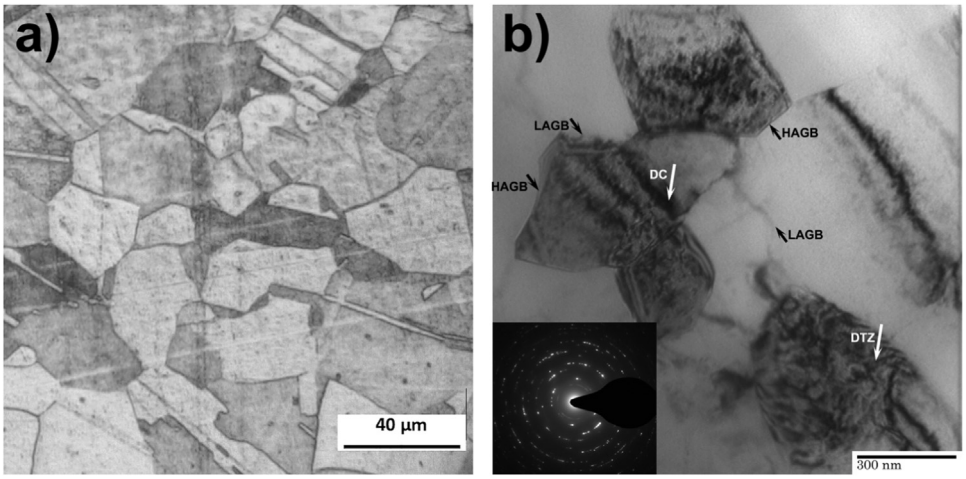

Fig. 6. (a) OM micrograph of the annealed Cu and (b) TEM microstructure of C6 matrix with the corresponding SAD pattern. High-angle grain boundaries (HAGBs) and low-angle grain boundaries (LAGBs), dislocation cell (DC), and dislocation tangle zones (DTZ) are shown in the TEM micrograph.

(evaluated by the line intercept method) are approximately 31 and 0.34 μm, respectively. Therefore, the application of six ARB cycles leads to a substantial microstructural refinement. It is noticeable that other researchers have reported comparable grain sizes for six cycles ARB processed Cu in the monolithic condition [5,29]. It has been shown that in the case of metallic materials having medium to high stacking fault energy, the dislocation activity significantly controls the grain refinement behavior [30]. The grain refinement mechanism of Cu includes the following steps of i) the creation of low-angle grain boundaries in the form of subgrains and dislocation cells via propagation, interaction and rearrangement of dislocations, ii) the gradual increment of the boundary misorientation to form high-angle grain boundaries (HAGBs) from low-angle grain boundaries (LAGBs) because of the accumulation of dislocations and iii) the migration of HAGBs [31]. Also, it has been reported that in the case of Cu, the recrystallization phenomenon could annihilate dislocations by increasing the ARB passes [32]. The high density of dislocations (as the main lattice defect), generated and accumulated by SPD is the main driving force for Cu matrix recrystallization. On the other hand, the high purity of the metallic material besides deformation adiabatic heating could facilitate and accelerate recrystallization. Regarding Fig. 6b, the co-existence of bright (dislocation free) and dark (dislocation cell and tangle zones) grains approves the occurrence of partial recrystallization. The co-operation of these two reverse phenomena (dislocation generation and annihilation) results in the development of a steady-state UFG microstructure finally. As indicated typically in the micrograph, although both HAGBs (sharp interface) and LAGBs (wavy and not well delineated) are clearly observable, the corresponding SAD pattern with the spotty ring shape confirms the co-existence of both HAGBs and LAGBs.

The micro-hardness variations of the monolithic Cu and Cu/B_4C composite materials are plotted in Fig. 7. It should be mentioned that zero cycle corresponds to the annealed Cu. As it can be seen, the hardness of the monolithic Cu was enhanced up to three cycles and then saturated. The hardness saturation of the monolithic Cu after three ARB cycles has been previously reported [30]. Therefore, it is believed that the strain and grain boundary hardening are the main affective mechanisms. The first one is dominant in the initial stages of deformation owing to the dislocations generation, interaction, pinning, and finally their mobility reduction [33]. It has been reported that the dislocation density of Cu was significantly enhanced (approximately 5000%) and then quickly saturated after one pass of ARB [34]. The initial high rate of the hardness enhancement shows the strong influence of this mechanism on the material hardening. Thereafter, the second mechanism which is based on dislocation rearrangement

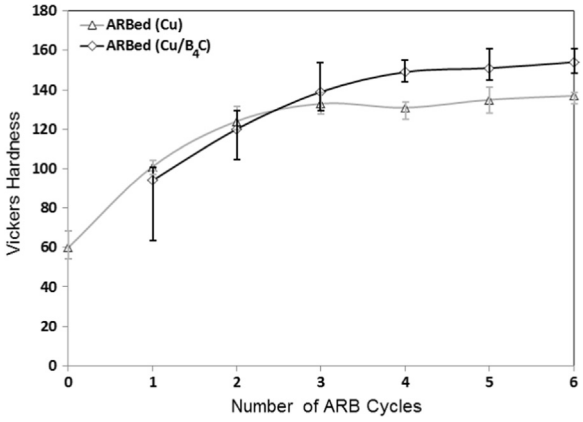

Fig. 7. Vickers microhardness of the monolithic and composite materials processed at different ARB cycles.

and migration plays the main role in the hardness enhancement. The comparison of the hardness variation of the composites and monolithic Cu demonstrates the lower and higher hardness values of the composites to two cycles and after three cycles, respectively. Another difference is the unsaturation of the composite's hardness by continuing the ARB process up to the last cycle. As well as those two mentioned mechanisms, the dispersion hardening could be an operative mechanism in the case of the Cu/B_4C composite material. As displayed previously, in the initial cycles of the composite production by ARB, the ceramic particles become agglomerated in the bundles between the Cu layers. In this condition (intense agglomeration), dispersion hardening is not an operative strengthening mechanism. Moreover, according to the film theory, the existence of the ceramic bundles between the Cu layers decreases the metallic layers bond strength (with respect to the monolithic ARBed Cu) [35,36], and makes a partially delaminated material in the initial ARB cycles. Moreover, the agglomerated particles outpour from the interfacial ceramic bundles during the sample preparation (polishing) because of the low reinforcement-matrix bonding quality (Fig. 3b). These explain the lower hardness values and higher standard deviations of the composites compared to the fully bonded dense ARBed monolithic Cu sample in the initial ARB cycles. This is consistent until the ceramic bundles fragment dispersed to some extent, and also the Cu layers bonding quality was improved (due to a higher reduction in thickness), starting in the 3rd ARB pass. Although after three ARB cycles the hardness of the Cu matrix was saturated due to relative microstructural stabilization, the role of the ceramic particles in the hardness enhancement was significant hereafter. This

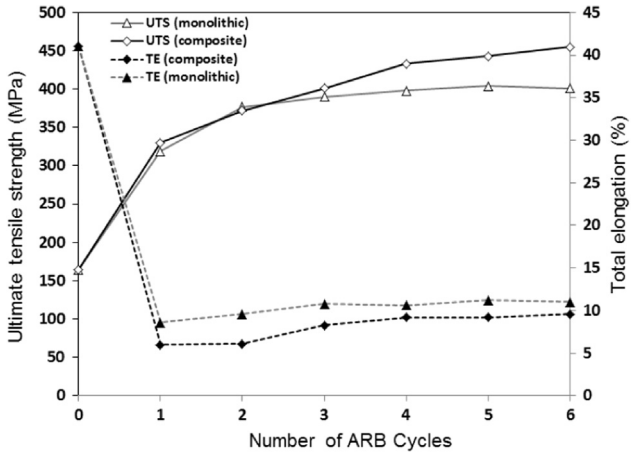

Fig. 8. UTS and TE values of the monolithic Cu and Cu/B_4C composite materials.

could explain why the hardness of the composite is continuously enhanced up to the last ARB cycle. This leads to over 30% increment in hardness (with respect to ARBed monolithic Cu) after six processing cycles.

Fig. 8 indicates the ultimate tensile strength (UTS) and total elongation values of the composite and monolithic Cu materials processed at different ARB cycles. Similar to the hardness variation, the curve of the monolithic ARBed Cu reached a plateau after three cycles. As can be seen, ~140% increment in strength was obtained with respect to the annealed Cu. The coincidence of the hardness and strength saturation could be justified regarding the direct relation of the hardness and strength in metallic materials [37]. Concerning the diagram, after three ARB cycles, the UTS curve of the composite surpasses from the corresponding curve of the monolithic Cu and keeps its incremental tendency, similar to the hardness variation curves. The development of the particles dispersion and structural uniformity, the enhancement of the Cu layers' bond strength as well as the elimination of porosity by increasing the ARB cycles are the main reasons for the positive slope of the UTS curve in the case of the composite material up to the last pass. The diagram shows 175% improvement in UTS after six cycles of ARB in comparison to the annealed material. Considering the total elongation variations, after one ARB cycle, the substantial reductions of total elongation from 41% to 8.6% and 6% were observed in the monolithic and composite materials, respectively. These could originate from strain hardening of the materials as well as weak bonding between the layers. Obviously, in each ARB cycle, the total elongation values of the composites are lower than those of the monolithic materials. In the composite samples, lower bonding strength between the Cu layers and higher structural porosity, especially in the initial ARB passes existed. Such porosity or discontinuities change the local stress mode from 2D to 3D (because of the stress concentration) and consequently reduce the materials ductility and tensile strength simultaneously. Furthermore, even in the last ARB cycles, several ceramic-metal interphases as crack initiation locations existed within the composites. These may result in a lower strain endurably of the composites with respect to the monolithic samples in all ARB cycles. In addition to the layers bond strength enhancement and internal porosities decrement, it has been reported that the development of recrystallization in Cu by increasing the deformation strain or ARB cycle leads to a ductility enhancement in ARBed monolithic metals [30]. In the case of the ARBed composite material, a better particle dispersion and homogeneity improvement by continuing ARB have positive influences on the ductility enhancement as well.

The fracture surfaces of the C2, C4 and C6 specimens are displayed in Fig. 9. The C2 sample clearly shows disjoined Cu layers. As a consequence, each layer tolerates load independently. As it was previously discussed, in this situation, the particles could not reinforce

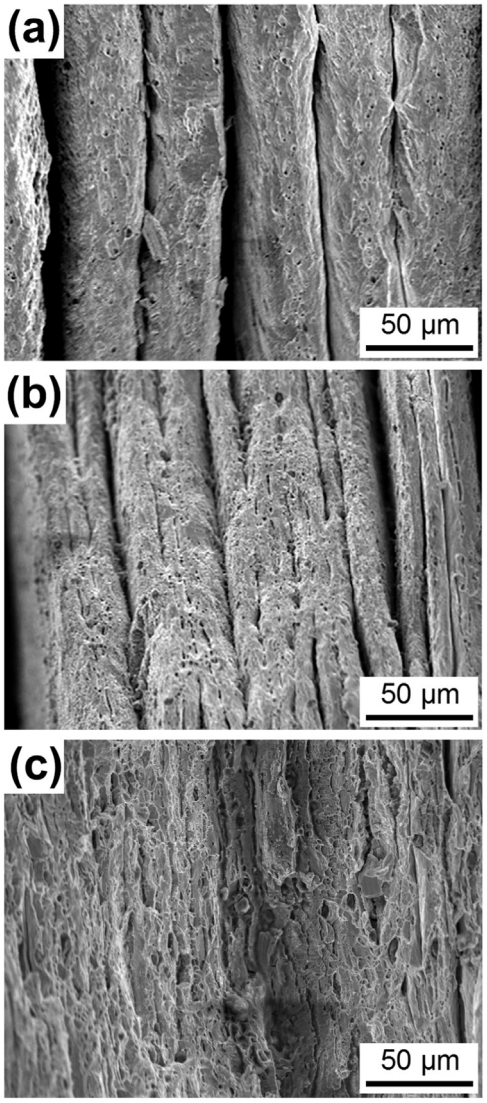

Fig. 9. Fracture surfaces of the composites: (a) C2, (b) C4 and (c) C6.

the material. By increasing the ARB cycle, some bonded and de-bonded layers are present concurrently (C4). Therefore, the reinforcing role of the ceramic particles is local and incomplete. As it can be seen, continuing the ARB process to six cycles (C6) results in fully bonded layers. In such enbloc material, the ceramic reinforcements perform their role efficiently. These images can be also used to support the previous discussions.

Fig. 10 demonstrates the high-magnification fractographs of the C2, C4, C5 and C6 samples. The presence of dimples confirms the occurrence of ductile rupture in all of the samples. The ejection of particles from interfacial bundles is clear in C2. As indicated in the images by ovals the particle agglomerated zones were observable in the C4 and C5 specimens. By increasing the ARB cycle, the size of the particle agglomeration zones was reduced and the particles were dispersed more uniform as far as no agglomeration zone was detectable in C6. Due to the higher strength of the UFG Cu matrix the de-cohesion of the matrix-reinforcement interphases is more likely than crack initiation within the matrix during the test. This confirms the existence of ceramic particles in the core of dimples (depicted by arrows) as crack initiation sites.

Fig. 11 shows the electrical resistivity (ER) variations of the ARBed Cu and Cu/B_4C materials at different cycles. In both of the material type, ER was generally enhanced by increasing the applied strain. In the case of monolithic Cu, the electrical resistivity value increases from

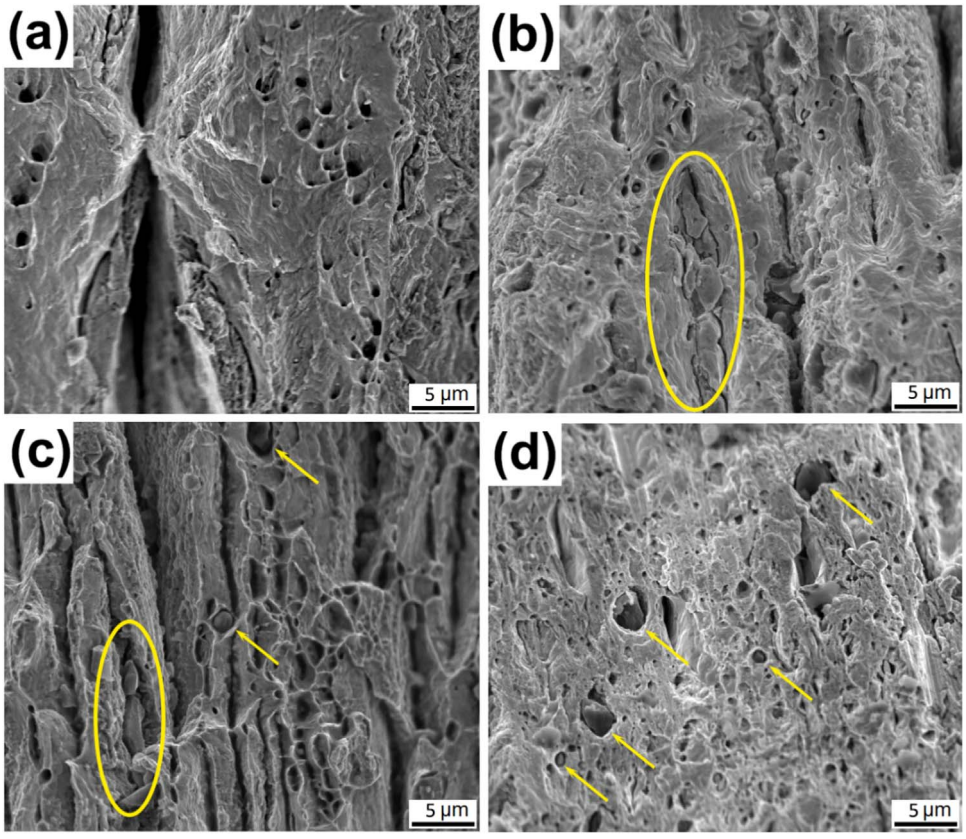

Fig. 10. High magnification SEM fractographs of the (a) two, (b) four, (c) five and (d) six cycles ARB processed Cu/B_4C composites. The arrows show particles in the core of dimples as crack initiation sites; also, the ovals indicate particle agglomerated zones.

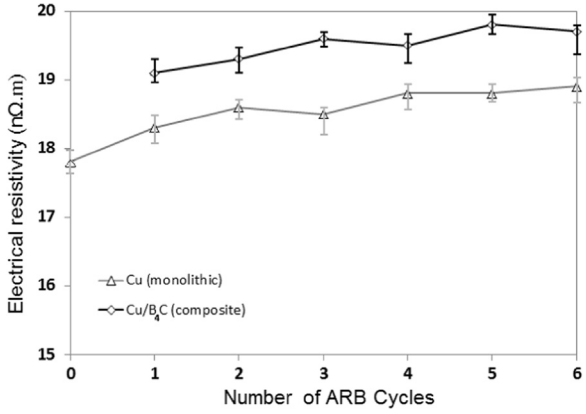

Fig. 11. ER of the ARBed monolithic and composite materials at different cycles.

17.8 nΩ m to ~18.9 nΩ m after six ARB cycles. Other studies have reported analogous changes in ER of commercial pure Cu alloys after SPD processing to similar strain values [5,38]. Various electron scattering mechanisms could alter ER of a SPDed monolithic metallic material. The resistivity increment due to phonons, impurities, grain boundaries and dislocations could be the major affective mechanisms [39]. Hereon, the influences of the first and second mechanisms are not remarkable due to the isothermal ER measurement and the application of highly pure Cu alloy, respectively. Also, it has been stated that the impact of dislocation scattering is not significant if the dislocation density was below 10^{17} m^{-2} [39]. Since the dislocation density of SPDed Cu are lower than that critical value (probably due to recrystallization) [34,40,41], this factor could be ignored as well. Consequently, it can be stated that such ER enhancement in monolithic Cu is solely owing to grain refinement originated from applied strains during ARB. It has been shown that if the grain size of a material was smaller than its electron mean free path, the ER increment of the material could be remarkable. Whereas the average grain size of the monolithic Cu is considerably higher than the Cu electron mean free path at room temperature (~40 nm [39]), a minor ER enhancement of the six cycles ARBed monolithic Cu with respect to the annealed sample is justifiable. Considering the ER variation of the Cu/B_4C composites, ER was enhanced to ~19.7 nΩ m after six cycles. In other words, ER of the materials was enhanced ~1.9 nΩ m in comparison to the annealed Cu. It the case of metal matrix composite materials an additional scattering factor could be affective on ER (beside the previous mechanisms), namely interface scattering [39]. However, this mechanism is not significantly operative here due to the content and shape of the reinforcement. The relatively low volume percentage and particulate shape of the reinforcement develop inconsiderable internal interphase boundary surfaces as well as a continuous conductive matrix. In general, this mechanism is significantly effective in the case of nano-laminate or multilayered composite materials when the conductive layer thickness is smaller than the electron mean free path of the metal [39]. Also, it has been shown that the overall saturated dislocation densities of Cu in the monolithic or composite conditions are not considerably different [42]. Since ARB is a solid-state and cold composite production method, no significant impurity was added to the Cu matrix during the process (unlike the liquid-state fabrication techniques of metal matrix composites). Therefore, the dislocation and impurities scattering mechanisms are not operative in the case of the composite materials. Consequently, it can be stated that the ER enhancement of the Cu/B_4C composites is merely owing to grain refinement and the inherent high electrical resistivity of B_4C, which decreases the conduction surface in a constant cross section of the specimen. Based on the Matthiessen's rule [39], the electrical resistivity induced by various independent electron scattering mechanisms is

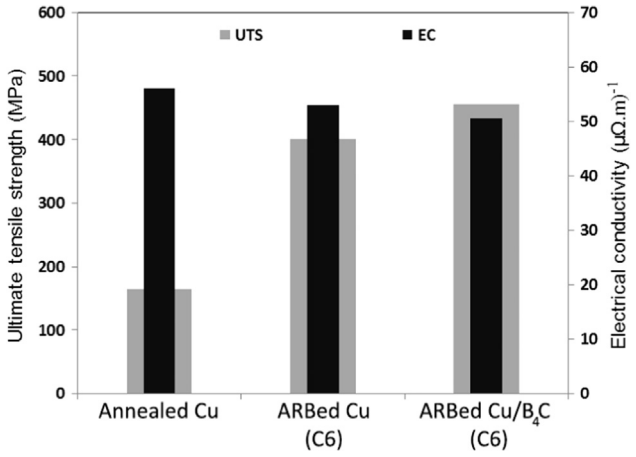

Fig. 12. UTS and EC comparison of the annealed monolithic Cu and six cycles ARB processed monolithic and Cu/B_4C composite materials.

equivalent to the summation of various individual electrical resistivity values made by each scattering mechanism. Considering this rule and the fact that the average grain size of the Cu matrix is similar to the monolithic Cu, the contribution of the ceramic particles in the ER enhancement of the composite is about 0.8 nΩ m (1.9–1.1 nΩ m). This is in accordance with the standard models proposed to evaluate the ER variation of the metal matrix composites [43,44].

For comparison, Fig. 12 demonstrates the UTS and electrical conductivity (EC) values of the annealed and strengthened Cu strips. As it can be seen, in spite of the considerable enhancement in UTS, a minor reduction in EC (inverse of ER) of the material was observed after six ARB cycles. This could originate from the difference of the operative mechanisms. Although the addition of the B_4C particulate ceramic during the ARB process after six cycles leads to 4.7% reduction in EC, it could concurrently improve the material's strength to 13.5% with respect to the ARBed monolithic Cu.

4. Conclusions

In the current research, the ARB process was used to produce Cu/B_4C composites. The microstructural investigation of the composites shows that the uniformity of the particle distribution within the Cu matrix is improved by increasing ARB cycles. The radial distribution function and degree of clustering quantitatively confirm the distribution improvement. The TEM micrograph confirms the formation of UFG microstructure within the Cu matrix. The microhardness and UTS evaluations of the monolithic Cu show a sharp increment and quick saturation by increasing ARB cycles, while the microhardness and UTS of the composites keep their incremental trend up to the last cycle. Dramatic decrements in ductility of the ARBed monolithic and composite materials after one ARB cycle are followed by minor increments up to the last cycle. The slight decrement in electrical conductivity of the composite materials processed by six ARB cycles has been observed, while the hardness and strength increments are considerable. This study shows that ARB is a promising method to produce high-strength, high-conductive Cu/B_4C composites.

References

[1] J. Emsley, Nature's Building Blocks: An AZ Guide to the Elements, Oxford University Press, Oxford, UK, 2011.
[2] A. Russell, K.L. Lee, Structure-Property Relations in Nonferrous Metals, John Wiley & Sons, Inc., Hoboken, New Jersey, USA, 2005.
[3] W.D. Callister, D.G. Rethwisch, Materials Science and Engineering: An Introduction, Wiley, New York, 2007.
[4] C.S. Çetinarslan, Mater. Des. 30 (2009) 671–673.
[5] N. Takata, S.-H. Lee, N. Tsuji, Mater. Lett. 63 (2009) 1757–1760.
[6] J. Zhang, L. He, Y. Zhou, Scr. Mater. 60 (2009) 976–979.
[7] O.F. Higuera-Cobos, J. Cabrera, Mater. Sci. Eng.: A 571 (2013) 103–114.
[8] R. Islamgaliev, W. Buchgraber, Y.R. Kolobov, N. Amirkhanov, A. Sergueeva, K. Ivanov, G. Grabovetskaya, Mater. Sci. Eng.: A 319 (2001) 872–876.
[9] R. Valiev, Nat. Mater. 3 (2004) 511–516.
[10] M. Alizadeh, E. Salahinejad, Mater. Sci. Eng.: A 595 (2014) 131–134.
[11] M. Alizadeh, E. Salahinejad, J. Alloy. Compd. 620 (2015) 180–184.
[12] A.W. Weimer, Springer Science & Business Media, 2012.
[13] A. Sokhansanj, A. Hadian, World Sci. (2012) 94–101.
[14] M. Alizadeh, Mater. Lett. 64 (2010) 2641–2643.
[15] M. Alizadeh, Mater. Sci. Eng.: A 528 (2010) 578–582.
[16] A.H. Yaghtin, E. Salahinejad, A. Khosravifard, Int. J. Miner. Metall. Mater. 19 (2012) 951–956.
[17] A. Yazdani, E. Salahinejad, Mater. Des. 32 (2011) 3137–3142.
[18] A. Yazdani, E. Salahinejad, J. Moradgholi, M. Hosseini, J. Alloy. Compd. 509 (2011) 9562–9564.
[19] H. Bai, N. Ma, J. Lang, Y. Jin, C. Zhu, Y. Ma, Mater. Des. 46 (2013) 740–745.
[20] R. Sathiskumar, N. Murugan, I. Dinaharan, S. Vijay, Mater. Des. 55 (2014) 224–234.
[21] T. Yenera, I. Altinsoya, S. Yenerb, G.C. Efea, I. Ozbeka, C. Bindala, Acta Phys. Pol. A 127 (2015) 1045–1047.
[22] H.D. Manesh, Mater. Sci. Technol. 22 (2006) 634–640.
[23] N. Jia, F. Roters, P. Eisenlohr, D. Raabe, X. Zhao, Acta Mater. 61 (2013) 4591–4606.
[24] A. Malin, M. Hatherly, Met. Sci. 13 (1979) 463–472.
[25] Y. Sun, N. Tsuji, H. Fujii, F. Li, J. Alloy. Compd. 504 (2010) S443–S447.
[26] M. Tayyebi, B. Eghbali, Mater. Sci. Eng.: A 559 (2013) 759–764.
[27] M. Reihanian, E. Bagherpour, M. Paydar, Mater. Lett. 91 (2013) 59–62.
[28] M. Shamanian, M. Mohammadnezhad, H. Asgari, J. Szpunar, J. Alloy. Compd. 618 (2015) 19–26.
[29] N. Tsuji, Y. Saito, S.H. Lee, Y. Minamino, Adv. Eng. Mater. 5 (2003) 338–344.
[30] R. Jamaati, M.R. Toroghinejad, Mater. Sci. Eng.: A 606 (2014) 443–450.
[31] A. Fattah-alhosseini, O. Imantalab, Y. Mazaheri, M. Keshavarz, Mater. Sci. Eng.: A 650 (2016) 8–14.
[32] N. Takata, K. Yamada, K.-i. Ikeda, F. Yoshida, H. Nakashima, N. Tsuji, Mater. Trans. 48 (2007) 2043–2048.
[33] A.S. Argon, Strengthening Mechanisms in Crystal Plasticity, Oxford University Press, Oxford, 2008.
[34] Y. Miyajima, S. Okubo, H. Abe, H. Okumura, T. Fujii, S. Onaka, M. Kato, Mater. Charact. 104 (2015) 101–106.
[35] M. Hosseini, H.D. Manesh, Mater. Des. 81 (2015) 122–132.
[36] M. Rezayat, A. Akbarzadeh, Mater. Des. 36 (2012) 874–879.
[37] P. Zhang, S. Li, Z. Zhang, Mater. Sci. Eng.: A 529 (2011) 62–73.
[38] K. Edalati, K. Imamura, T. Kiss, Z. Horita, Mater. Trans. 53 (2012) 123–127.
[39] L. Tian, I. Anderson, T. Riedemann, A. Russell, Acta Mater. 77 (2014) 151–161.
[40] J. Čížek, M. Janeček, O. Srba, R. Kužel, Z. Barnovská, I. Procházka, S. Dobatkin, Acta Mater. 59 (2011) 2322–2329.
[41] J. Gubicza, L. Balogh, R. Hellmig, Y. Estrin, T. Ungár, Mater. Sci. Eng.: A 400 (2005) 334–338.
[42] J. Verhoeven, H. Downing, L.S. Chumbley, E. Gibson, J. Appl. Phys. 65 (1989) 1293–1301.
[43] S.-Y. Chang, C.-F. Chen, S.-J. Lin, T.Z. Kattamis, Acta Mater. 51 (2003) 6291–6302.
[44] L. Weber, J. Dorn, A. Mortensen, Acta Mater. 51 (2003) 3199–3211.